Nonlinear Dynamics (2026) 114:258
https://doi.org/10.1007/s11071-025-12126-8

RESEARCH

Identification of nonlinear frequency response curves under shaker-structure interaction through force-controller-free phase-locked loop testing

Zoltan Gabos[1,2] · G. Raze[3] · G. Kerschen[3] · Zoltan Dombovari[1,2]

Received: 16 June 2025 / Revised: 2 October 2025 / Accepted: 5 December 2025

Abstract
This paper presents an integrated approach for extracting nonlinear frequency response (NLFR) curves in systems affected by shaker-structure interaction. The approach leverages three distinct phase-locked loop (PLL) testing methods, each tailored for different levels of coupling effects. By resectioning the response surfaces obtained from the proposed PLL-based tests, the need for force controllers is eliminated. The technique is validated through numerical and experimental studies. Experiments conducted on nonlinear beam and plate structures illustrate the effectiveness of the proposed technique, even in the presence of coupled modes.

Keywords Nonlinear vibration · System identification · Signal processing · Coupled dynamics · Phase-locked loop testing

1 Introduction

Modern engineering practices heavily rely on vibration testing for the experimental identification of structural and component parameters. In the case of linear systems, experimental modal analysis is a widely used approach [10, 15]. However, for nonlinear systems, the principle of superposition, fundamental to modal testing, no longer holds. As engineering design trends shift toward increasingly complex and slender geometries, nonlinear phenomena have become more prevalent in practical applications [20, 24]. Structures particularly susceptible to nonlinear behavior include microelectromechanical systems (MEMS) [26, 38], wind turbines and turbo machinery [18, 31], commercial aircraft or spacecraft [4, 25], and thin-walled structures [5, 35].

✉ Zoltan Gabos
zoltan.gabos@mm.bme.hu

[1] Department of Applied Mechanics, Faculty of Mechanical Engineering, Budapest University of Technology and Economics, Műegyetem rkp. 3, Budapest 1111, Hungary

[2] MTA-BME Lendület Machine Tool Vibration Research Group, Department of Applied Mechanics, Budapest University of Technology and Economics, Budapest 1111, Hungary

[3] Space Structures and Systems Laboratory, Aerospace and Mechanical Engineering Department, University of Liege, Liège, Belgium

The growing prevalence of nonlinear behavior in vibrating structures has driven extensive research aimed at understanding their rich and complex dynamics [20, 24, 29]. A fundamental approach to characterizing and understanding vibrating systems is through their frequency response curve, a concept that extends naturally to nonlinear structures. We define the nonlinear frequency response (NLFR) curves to describe the system's response amplitude and phase lag as functions of the forcing frequency for a given constant forcing amplitude. While the frequency response of a nonlinear system primarily aids engineering interpretation, the force-normalized linear frequency response function (FRF) [10, 15] remains a direct tool for estimating linear system parameters and complex system responses. Several analytical methods, including the method of multiple scales [14, 23], Lindstedt-Poincaré [14, 23], and harmonic balance [14, 23], are well-established for deriving NLFR curves, alongside numerical continuation techniques [7, 9]. To generalize the concept of normal modes in nonlinear systems, nonlinear normal modes (NNMs) have been defined either as the periodic orbits of an undamped and unforced system [30] or as invariant manifolds in phase space [32]. Additionally, reduced-order modeling techniques [36] and the definition of spectral submanifolds [28] have been introduced to further refine the analysis of nonlinear vibrations.

While analytical and numerical methods for studying nonlinear dynamics are well-established, experimental approaches

Published online: 24 February 2026

remain under continuous development and refinement [29]. A common and straightforward technique for extracting NLFR curves from measurements involves open- or closed-loop sweeps of excitation frequency [13, 29]. More advanced control-based methods [2], such as control-based continuation (CBC) [3, 6, 33], response-controlled stepped-sine excitation testing [19], and phase-locked loop (PLL) testing [8, 34], have also been developed. These methods are actively researched to enhance their applicability in industrial testing. Although an initial approach for systematically approximating control parameters has been proposed [17], most of these methods still lack algorithmic parameter tuning. As a result, their implementation remains a largely heuristic and time-consuming process, relying heavily on expert intuition and experience.

Beyond optimizing the control parameters of the methods above, another major challenge is shaker-structure interaction [13, 37, 40], particularly in PLL testing, where the phase lag of the forcing and the structure's response is controlled continuously. By incrementing the phase lag (control target) in time and collecting the response amplitude, forcing amplitude, and forcing frequency data, one can map the NLFR curves directly from PLL tests. We consider shaker-structure interaction relevant when there is a significant mechanical coupling between the structure and the dynamics of the shaker. This interaction is most pronounced at resonances, where the so-called force drop-off phenomenon occurs [37], causing the system's response to correspond to varying forcing amplitudes. While this effect is inconsequential in linear systems, where it primarily affects the signal-to-noise ratio and FRFs remain invariant with respect to the input force, it poses a significant issue in nonlinear system identification. As a result, the extracted curves deviate from the true NLFR [13], as will be clearly demonstrated in this study. Although incorporating force amplitude control alongside PLL is an appealing solution [1], determining the appropriate controller gains remains a heuristic process. Moreover, the force controller might reach the power limitation available to the shaker. Consequently, force controllers may still exhibit variation in amplitude with respect to the forcing frequency. Note that in this study we distinguish between two separate forcing-related amplitudes: one associated with the driving signal amplitude F_0, and the other corresponding to the measured physical input force $F_{\mathrm{i},1}$ at the excitation point. While the former F_0 is usually kept constant during open-loop practices, $F_{\mathrm{i},1}$ can vary with the forcing frequency. It is important to keep in mind the difference between F_0 and $F_{\mathrm{i},1}$, as we extensively rely on this key information in this study.

The force drop-off phenomenon is observed in open-loop frequency sweep experiments. In [13], it was shown that NLFR curves can be extracted from open-loop sine sweeps, even in the presence of shaker-structure interaction. This was achieved by sectioning the surface generated from the measured data at constant input forcing amplitudes $F_{\mathrm{i},1}$, a process known as resectioning. However, the resectioning approach in [13] was limited to capturing only the stable periodic orbits. An important contribution of the present study is the extension of this approach to PLL-based testing, which enables tracing of the complete surface, including both stable and unstable periodic orbits. Such a procedure provides a full picture of the structural dynamics and accurate boundaries of the bistable regions. We provide a detailed guideline on selecting the appropriate methods based on the magnitude of shaker-structure interaction. These methods comprise the phase-locked loop frequency sweep (PLL-FR), which varies the phase lag at constant F_0 values, resectioning of PLL-FR results, and a phase-locked loop input force sweep (PLL-IF) test, where F_0 is continuously increased at constant phase lag values (and it is assumed that $F_{\mathrm{i},1}$ is growing with F_0). Note that these three schemes do not affect the input force amplitude and do not involve the use of a force control scheme. Furthermore, we highlight the potential ineffectiveness of force controllers in PLL testing (PLL-FC), which aims to maintain a constant forcing amplitude, reinforcing the advantages of our proposed approach. This limitation of force controllers for nonlinear structures has also been observed in commercial solutions such as TestLab [19]. Additionally, continuous force control remains primarily the subject of academic research [16, 39] rather than general engineering practice. Finally, while we acknowledge that shaker-structure interaction can introduce harmonic distortion in the forcing signal [16], this study focuses specifically on the force drop-off phenomenon.

The remainder of this study is structured as follows. Section 2 introduces the shaker-structure interaction problem using the simplest two-degree-of-freedom (2-DoF) extension of the single DoF Duffing oscillator by an additional DoF, describing the shaker. Section 3.1 provides a detailed explanation of the PLL-FR method, including the optional use of a force controller. In Sect. 3.2, we present the proposed guidelines and demonstrate their application through a 2-DoF numerical case, illustrating how NLFR curves can be extracted from measurements while accounting for shaker-structure interaction, without requiring a force controller. This section also discusses the limitations of the resectioning approach, particularly regarding the forcing range covered during PLL-FR or PLL-IF tests. Next, Sect. 4 presents experimental validations using a nonlinear beam and a thin metal plate, similar to those examined in [20, 29]. Finally, Sect. 5 provides a summary of our findings and concluding remarks.

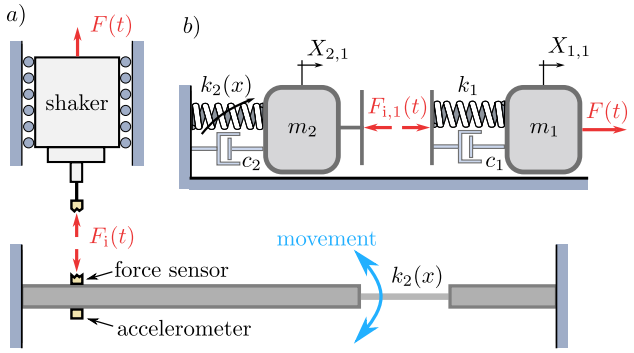

Fig. 1 Sketch of the structure (**a**) and the 2 DoF model (**b**), used for the numerical demonstration in this study. (**b**) is a simplified model of a beam structure (**a**) with geometric nonlinearity, forced by an electrodynamic shaker. The force-drop-off phenomenon occurs due to the coupling of the exciter and the tested system

2 Problem formulation: shaker-structure interaction

In this section, the force variation and its consequences are demonstrated using a 2 DoF nonlinear oscillator modelling shaker-structure interaction [13] as seen in Fig. 1.

$$\begin{bmatrix} m_1 & 0 \\ 0 & m_2 \end{bmatrix} \begin{bmatrix} \ddot{x}_1 \\ \ddot{x}_2 \end{bmatrix} + \begin{bmatrix} c_1 & -c_1 \\ -c_1 & c_1 + c_2 \end{bmatrix} \begin{bmatrix} \dot{x}_1 \\ \dot{x}_2 \end{bmatrix} + \begin{bmatrix} k_1 & -k_1 \\ -k_1 & k_1 + k_2 \end{bmatrix} \begin{bmatrix} x_1 \\ x_2 \end{bmatrix} + \begin{bmatrix} 0 & 0 \\ 0 & m_2 \mu \end{bmatrix} \begin{bmatrix} 0 \\ x_2^3 \end{bmatrix} = \begin{bmatrix} F(t) \\ 0 \end{bmatrix}, \quad \text{with} \quad F(t) := F_0 \cos \omega t, \tag{1}$$

where $F_0 > 0$ and m_1 represents the mass of the moving armature in a shaker. The excitation (input) force F_i (2) is driven into the structure through k_1 and c_1 combined stiffness and damping of the armature membrane and suspension of the shaker. The parameters m_2, k_2, c_2 and μ are the apparent mass $m_{\mathrm{AA}} =: m_2$, stiffness $k_{\mathrm{AA}} =: k_2$, viscous damping and nonlinear parameter $\mu_{\mathrm{AA}} =: \mu$ of the nonlinear structure, respectively. Here, the index AA denotes that the excitation and measurement points are the same on the tested structure. The forcing frequency ω and the driving force amplitude F_0 can be independently set. The values used for the numerical simulations are listed in Table 1 and correspond to those of the measured beam structure discussed later in Sect. 4.1. The visual representation of the system can be seen in Fig. 1.

In the mechatronic system (1), x_1 and x_2 represent the armature displacement of the shaker and the structure, respectively. The shaker's armature is directly excited by an electromagnetic driving force F_0, which is transmitted to the structure through a spring-damper system, generating the connection (input) force

$$F_\mathrm{i} = k_1 (x_1 - x_2) + c_1 (\dot{x}_1 - \dot{x}_2), \tag{2}$$

that excites the structure. The following descriptions of the main harmonics in the measured signals are defined as

$$x_2(t) =: \sum_{l=-\infty}^{\infty} X_l \, \mathrm{e}^{l\omega i t}, \quad F_\mathrm{i}(t) =: \sum_{l=-\infty}^{\infty} F_{\mathrm{i},l} \, \mathrm{e}^{l\omega i t}, \tag{3}$$

where X_1 and $F_{\mathrm{i},1}$ are the fundamental harmonics of the structure response $x_2(t)$ and the input force $F_i(t)$. In a practical test, this force is measured, but it cannot be directly assigned. As the excitation frequency or amplitude varies, the connection (input) force F_i undergoes complex changes, leading to the phenomenon of force (variation) drop-off at the resonance. In fact, simulations involving up-and-down frequency sweeps on the system (1) produce the results shown in Fig. 2. Contrary to our engineering intuition, the applied input force amplitude $|F_{\mathrm{i},1}|$ on the second moving mass m_2 (representing the structure), is not constant and can show hysteretic behavior at large driving force signal amplitudes F_0, similar to the response amplitude. While Fig. 2a shows how the input force amplitude applied to the structure differs from the constant case, panel b) demonstrates the deviation between the sweeps and the equivalent, ideal 1 DoF (Duffing) system, traced by the COCO software [7]. The parameters of the 1 DoF system without the mechanical coupling of the shaker,

$$m\,\ddot{x} + c\,\dot{x} + k\,x + \beta\,x^3 = F(t), \tag{4}$$

are listed in Table 1. Note that the linear stiffness and damping values are slightly different from those of the mechatronic system (1). This is due to the coupling effect that shifts the apparent modal parameters of a physical structure toward the shaker's dynamics. Note that changing the system parameters will result in different curves, but the conclusions drawn in this study will remain valid. As an example, Fig. 2c and d show the coupled dynamics of the same system, but with softening nonlinear characteristics. Although a significant difference with Fig. 2a and b can be observed, this example can still be treated with the approach proposed in this paper, as discussed in Sect. 4.3.

Phase-locked loop frequency sweep (PLL-FR) tests can also be performed on system (1), as illustrated in Fig. 2. While the complete curves can be obtained from these sweep simulations without the occurrence of the jump phenomenon, they do not accurately represent the NLFR curves and thus cannot be relied upon for parameter extraction and engineering decision-making. Both the sweeps and PLL-FR tests significantly differ from the NLFR curves, resulting in misleading results. This discrepancy serves as the primary motivation

Table 1 Parameters of the 2 DoF and 1 DoF nonlinear systems, representing the same vibration mode with the same forcing parameters

2 DoF nonlinear system						
m_1 (kg)	k_1 (N/m)	c_1 (Ns/m)	m_2 (kg)	k_2 (N/m)	c_2 (Ns/m)	μ (N/kg/m^3)
0.05	2630	30	1.53	57750	16	$4 \cdot 10^{10}$
1 DoF (Duffing) nonlinear system						Driving force
m (kg)	k (N/m)	c (Ns/m)	$\mu_0 = \beta/m$ (N/kg/m^3)			$\omega \in [180,\ 240]$ rad/s
1.53	57850	16	$4 \cdot 10^{10}$			$F_0 \in [0.1,\ 3.1]$ N

The parameters are related to those of the beam structure considered in Sect. 4.1

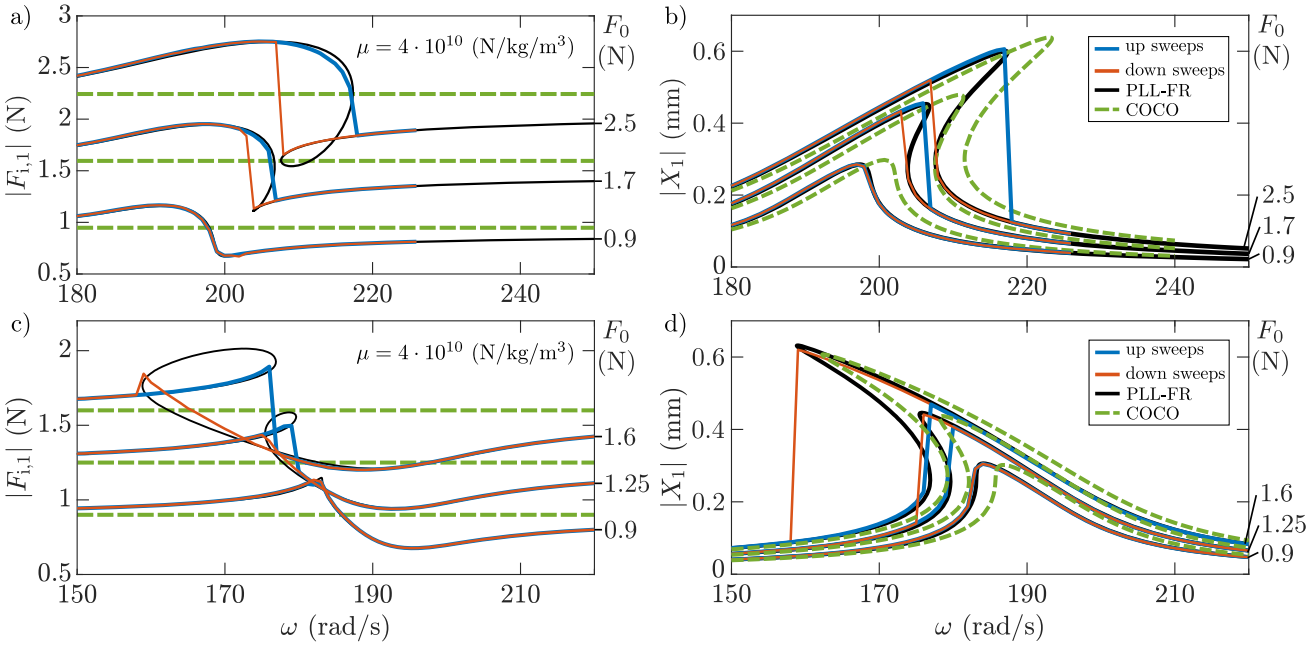

Fig. 2 Input force, $|F_{i,1}|$ (variation) drop-off phenomenon in the 2 DoF nonlinear oscillator. Top row: hardening nonlinearity; bottom row: softening nonlinearity. Only the nonlinear parameter μ differs between the two rows. **a** and **c** Frequency-dependent input force amplitude during simulated frequency sweep and simulated PLL-FR tests; **b** and **d** Consequences of the input force variation compared to the ideal single DoF Duffing system traced by COCO, where the excitation force is constant

for the research presented here. Our objective is to address the misleading outcomes caused by the input force drop-off phenomenon during PLL-FR testing, all without relying on force controllers.

Although the results from the sweep and PLL-FR tests produce curves that differ from the expected NLFR curves, when visualized in the excitation frequency-input force amplitude-response amplitude space, they trace the same surface. This observation is crucial for our approach, which involves sectioning this surface at constant input force amplitudes. The PLL-FR traced NLFR surface is shown in Fig. 3a, along with its corresponding projections (black) and the resectioned NLFR curves (red) in panels b), c) and e). Additionally, the input force drop-off phenomenon induced deformation of the phase, and the force normalized responses are visualized in Fig. 3d and f, respectively. Note that only the pointwise input force-normalization can be executed along the frequency, due to the intrinsic nonlinear and non-constant input force amplitude nature of the problem, meaning that the measured data points on the NLFR curves have to be normalised by the measured input force amplitudes at those points. The input force-normalised response, also known as nonlinear FRF [20] or quasi-FRF (QFRF) [11], can only be used for engineering comprehension or decision-making, unlike for response derivation from FRFs in linear cases.

In the remainder of this paper, we present an integrated technique to address the issues arising from the shaker-structure interaction discussed in this section.

3 Measurement technique

This section offers a comprehensive description of the methods used, along with the integrated technique that facilitates

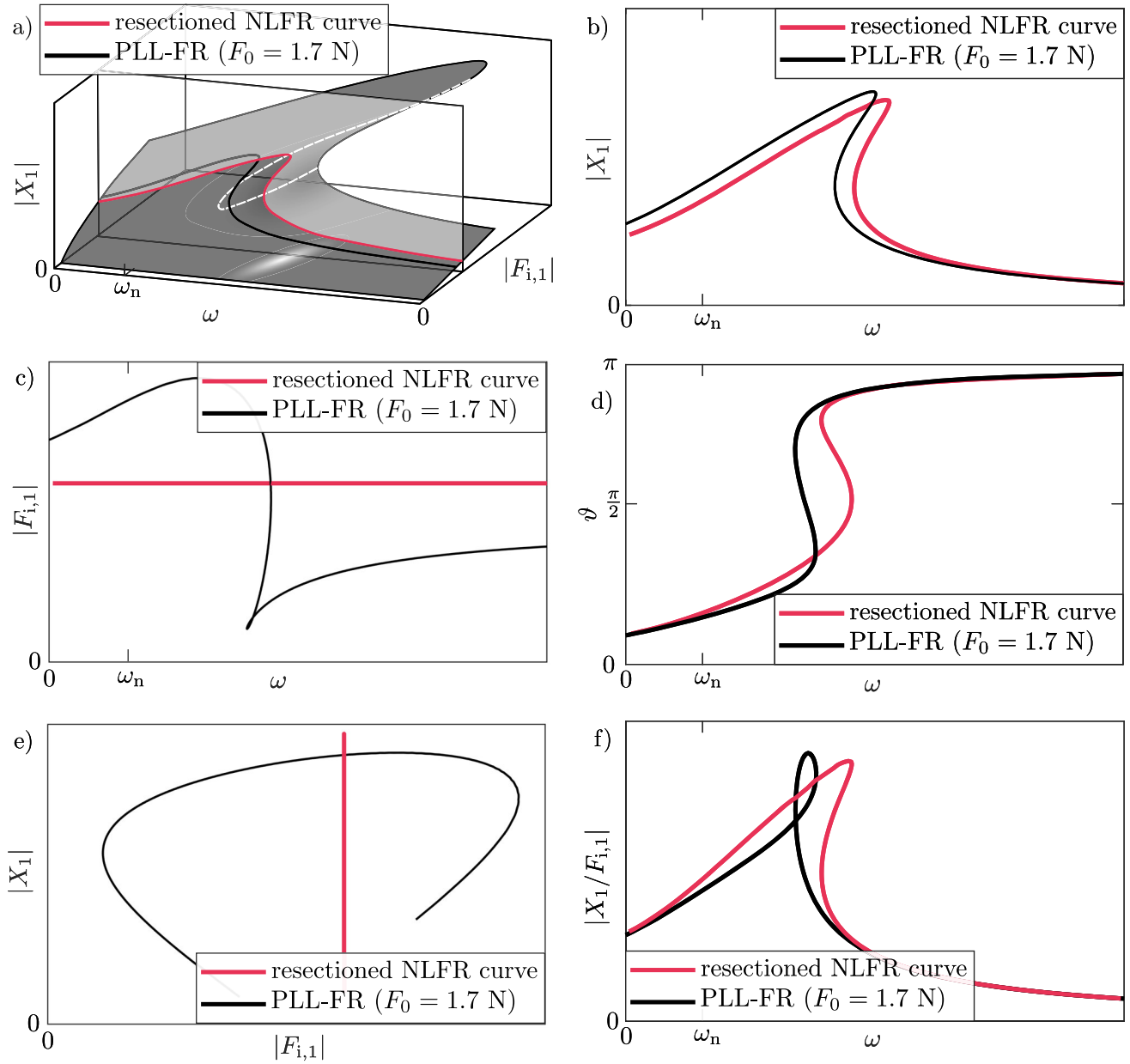

Fig. 3 Input force, $|F_{i,1}|$ drop-off phenomenon when using PLL-FR testing. **a** NLFR surface with a single PLL-FR test and the section at constant input force amplitude; **b**, **c** and **e** comparison of the two curves with different view angles. Panels **d** and **f** demonstrate the difference between the PLL-FR test and the section for the phase (**d**) and the normalized response curves (**f**)

the effective extraction of NLFR curves in the presence of shaker-structure interaction during testing. We begin by briefly summarising the PLL-FR and PLL-IF techniques, followed by an introduction to the PLL method, and finally, the proposed integrated testing technique.

– **PLL-FR**: phase-locked loop frequency sweep testing meaning the experimental continuation of NLFR curves $\omega - X_1$, where the phase lag ϑ is continuously varied by varying excitation frequency ω at constant driving force amplitudes F_0.
– **PLL-IF**: phase-locked loop input force sweep testing meaning the experimental continuation of $F_{i,1}$-X_1 curves, where the driving force amplitude F_0 is continuously varied at constant phase lags ϑ.

These methods directly result in the surfaces $X_1 - \vartheta - F_0$ and $X_1 - \omega - F_{i,1}$, discussed in this section.

3.1 Phase-locked loop method (PLL)

In this study, the extraction of NLFR curves is executed through the PLL testing of systems with apparent shaker-structure interaction. The phase-locked frequency sweep (PLL-FR) method is facilitated by the relation between the phase lag ϑ and the forcing frequency ω. Thus, the natural continuation can be applied on the parameter ϑ, leading directly to the NLFR curves [2, 8, 21, 27]. However, the dynamics of the forcing (e.g. electrodynamic shaker) always introduce coupled effects to some extent, even in the case of an input force amplitude controlled (PLL-FC) tests. The input force drop-off phenomenon will occur around resonance, leading to non-ideal response curves that are not representatives of the NLFR curves due to the non-constant input force amplitude, as illustrated in [13] and in Sect. 2.

The key objective of this work is to introduce an integrated technique for extracting NLFR curves by performing force controller-free PLL-FR measurements. This control-based method stabilizes unstable periodic orbits through a non-invasive control strategy, unlike CBC methods [3]. While the addition of a force controller is a straightforward and commonly used approach in the literature on PLL testing [1], it is not always effective when significant coupling effects are present, as will be discussed in Sect. 4.

The general concept of a PLL feedback control loop is discussed in a number of studies [8, 17, 34, 41]. We refer to study [41] for a block diagram of the control scheme (with an adaptive filter used for the real-time Fourier decomposition). The PLL method comprises a proportional-integral (PI) controller for the correction of the forcing frequency, a voltage-controlled oscillator (VCO) to generate the input force signal, and a phase detector to calculate the difference between the target phase ϑ_c and the phase lag ϑ. Additionally, a force controller is introduced for the output signal amplitude to illustrate the force-controlled case, in contrast to our proposed approach.

The continuation as a function of the variable ϑ and the stabilization of the unstable periodic orbits are ensured by a PI controller, similarly to the one in [41]:

$$\omega(t) = \omega_0 + k_\mathrm{P}\left(\vartheta_\mathrm{c} - \vartheta(t)\right) + k_\mathrm{I}\int_0^t \vartheta_\mathrm{c} - \vartheta(\tau)\,\mathrm{d}\tau. \tag{5}$$

Here, ω_0 is the initial excitation frequency, and the parameters k_P and k_I are the proportional and integral controller gains, respectively. Finding the optimal values is primarily heuristic and can be cumbersome. We recommend first increasing k_I to quickly reach the target value, followed by adjusting k_P to ensure stability. Note that the PLL controller scheme does not affect the input force amplitude, and does not perform force control.

From the controlled frequency $\omega(t)$, a VCO generates the sinusoidal signal by integrating $\omega(t)$. This generates the phase change, also used in the phase detector, ensuring a smooth data extraction. The phase detector can operate offline by sampling signals from the ongoing measurement and calculating the necessary Fourier coefficients. However, this approach results in longer test durations, and transients after each step must dissipate before sampling can occur. Alternatively, phase detection can be performed using online techniques, as demonstrated in [8, 41]. In this work, we use the adaptive filtering method [3, 41], which continuously computes the Fourier coefficients during the measurements. The core idea is to assume that the measured signal has the form:

$$\hat{s}(t) = \mathbf{w}^\mathsf{T}(t)\,\mathbf{q}(t), \tag{6}$$

where $\hat{s}(t)$ is the approximation of signal $s(t)$ that can be either the measured response or the input force. The vector $\mathbf{q}(t)$ defines the harmonics of the signal:

$$\mathbf{q}(t) = [\,1 \quad \sin\omega t \quad \cos\omega t \quad \sin 2\omega t \quad \cos 2\omega t \quad \ldots\,]^\mathsf{T}. \tag{7}$$

The weight vector $\mathbf{w}$ gives the Fourier coefficients:

$$\mathbf{w}(t) = \left[\,w_0 \quad w_{\mathrm{s},1} \quad w_{\mathrm{c},1} \quad \ldots \quad w_{\mathrm{s},i} \quad w_{\mathrm{c},i}\right]^\mathsf{T}, \tag{8}$$

where the indices in the weights (or Fourier coefficients) $w_{\mathrm{s},i}$ and $w_{\mathrm{c},i}$, $i \in \mathbb{N}^+$, $i \geq 2$ are corresponding to the harmonics of the signal. Note that for the continuation of the primary resonance with the PLL-FR, the first three elements of $\mathbf{q}(t)$ and $\mathbf{w}(t)$ are a sufficient description of the measured signal. Using the least mean squares (LMS) adaptive filtering algorithm [3], the weights can be updated at each sampling time instant. First, the error has to be estimated at the i^{th} time step:

$$\epsilon(t_i) = s(t_i) - \mathbf{w}^\mathsf{T}(t_i)\,\mathbf{q}(t_i). \tag{9}$$

Then, the updated weights are given as

$$\mathbf{w}(t_{i+1}) = \mathbf{w}(t_i) + \gamma\,\mathbf{q}(t_i)\epsilon(t_i), \tag{10}$$

at time step $i+1$. Parameter γ ensures the convergence of the LMS method. Note, that this parameter is usually very small ($\gamma < 0.1$) and the optimal value varies with the forcing level and the sampling frequencies [1].

From the estimated Fourier coefficients, the instantaneous phase between the input force and the response signal can be calculated, along with the amplitudes of the fundamental harmonics.

The input force F_i regarding its fundamental harmonics $F_{\mathrm{i},1}$ is used in the optional force controller (PLL-FC), which

is an integrator feedback control loop in the form of

$$F_{\mathrm{c},1}(t) = F_{\mathrm{c},1,0} + k_{\mathrm{I,F}} \int_0^t F_{\mathrm{i},1,0} - F_{\mathrm{i},1}(\tau)\,\mathrm{d}\tau, \tag{11}$$

where $F_0 := F_{\mathrm{c},1}(t)$ (see (1)) is the instantaneous driving force amplitude signal with the initial $F_{\mathrm{c},1,0}$ value, and $F_{\mathrm{i},1,0}$ is the target input force amplitude. If improperly tuned, the $k_{\mathrm{I,F}}$ integral gain can quickly destabilize the system and damage the measurement rig. We suggest starting with a very small control gain $k_{\mathrm{I,F}}$ and increasing it carefully until the desired effect has been achieved. We emphasise that this control law is only used in the PLL-FC technique.

The PLL-FR method works by setting the phase lag between the applied input force and the displacement, but the latter is rarely measured directly. Usually, accelerometers are used, and the displacement can be retrieved through double-time integration. This approach is associated with practical issues such as drifts due to acceleration offsets, but there exists a simpler alternative for stationary signals. Since the harmonics of the acceleration are out-of-phase with respect to the displacement harmonics by π, the PLL-FR with acceleration feedback can easily be implemented with a -1 gain applied to the acceleration signal.

Typically, the PLL-FR method is used for tracing the NLFR curves of a structure. However, tracing the NLFR surface by locking the phase lag at different values and performing input force amplitude sweeps with the phase held constant is also possible. This approach allows us to define the achievable minimum and maximum input force amplitude. We refer to this method as phase-locked loop input force-sweeps (PLL-IF), which is also employed in the proposed integrated technique. Notice that there is no force controller used in the PLL-IF approach. It is simply a sweep in the input force signal of the exciter, with the phase lag held constant during the sweep.

In the remainder of this paper, the introduced PLL-FR and PLL-IF methods are used for demonstrating the proposed integrated technique and the input force drop-off phenomenon. Additionally, the data extracted from PLL-FC measurements reveal a deviation in the input force amplitude, despite the application of the controller.

3.2 Integrated testing technique

The goal of this section is to establish a testing guideline based on the phase-locked loop frequency sweep (PLL-FR) and phase-locked loop input force sweep (PLL-IF) methods, without the use of a force controller. The concept of the integrated technique is as follows. Perform simple PLL-FR tests when the interaction between the structure and the shaker is negligible. If coupling effects are noticeable, apply resectioning to the PLL-FR test. Finally, use the PLL-IF method when coupling effects are strong. The technique is illustrated through a 2 DoF simulated example (mechatronic system (1) in Sect. 2), highlighting the advantages and limitations of the proposed methods. At the end of this section, a comprehensive guideline is provided, specifying which methods to use for various scenarios.

For the execution of PLL-FR and PLL-IF simulations using the mechatronic system (1), the parameters $k_{\mathrm{I}} = 70$ $1/\mathrm{s}^2$, $k_{\mathrm{P}} = 10$ 1/s at a sampling frequency of $\omega_{\mathrm{s}} = 100$ kHz, and $\gamma = 0.01$ were used.

The first approach to consider is performing PLL-FR measurements as a direct representation of the NLFR curves. This is valid only if the shaker-structure interaction is negligible, which might be achieved through careful shaker placement. It is known that minimal interaction occurs when the apparent mass of the structure is significantly larger than the shaker's moving mass [10]. However, achieving sufficient apparent mass is not always possible. Therefore, the initial step is to conduct PLL-FR tests at the desired driving force amplitudes and assess the amplitude deviation. As an engineering guideline, we recommend using the PLL-FR test results as NLFR curves only if the input force amplitude $|F_{\mathrm{i},1}|$ deviation remains negligible across all tests. It is important to note that this threshold can be adjusted for specific cases based on more or less strict engineering criteria.

If the input force amplitude deviation exceeds the expectations, the outcome of the PLL-FR tests does not correspond to NLFR curves. However, the measured curves still lie on the NLFR surface, which can be traced by gathering multiple PLL-FR tests with increasing driving force values (to the shaker), see Fig. 4 and [13]. Then, the built surface can be resectioned at the desired input force levels, resulting in the sought NLFR curves. Figure 4b shows the resectioned and raw PLL-FR test curves compared to the numerical continuation of the equivalent 1DoF (Duffing) model (of the mode, corresponding to m_2), described by the mechatronic system (1) with the parameters mentioned in Sect. 2. This result highlights that the resectioning of the surface indeed separates the shaker dynamics from the structure, giving the correct representation of the NLFR curves. In panel c), the resectioned phase lag is compared to the raw PLL-FR test curves. Although the difference between the PLL-FR tests and the resectioned curves might seem small, the input force-normalized response curves, show fundamentally different results in panel d).

Smooth interpolation of the measured data points is crucial for the accurate resectioning of the NLFR surface. We consider two different approaches. The first approach simply interpolates the $\omega - X_1 - F_{\mathrm{i},1}$ and $\omega - \vartheta - F_{\mathrm{i},1}$ surfaces with $F_{\mathrm{i},1}$ as the interpolated value (direct interpolation) as in Fig. 5a and b. Although this approach is easily applicable to the traced NLFR surface, the scarcity of data in some regions can compromise the surface interpolation and, hence, NLFR

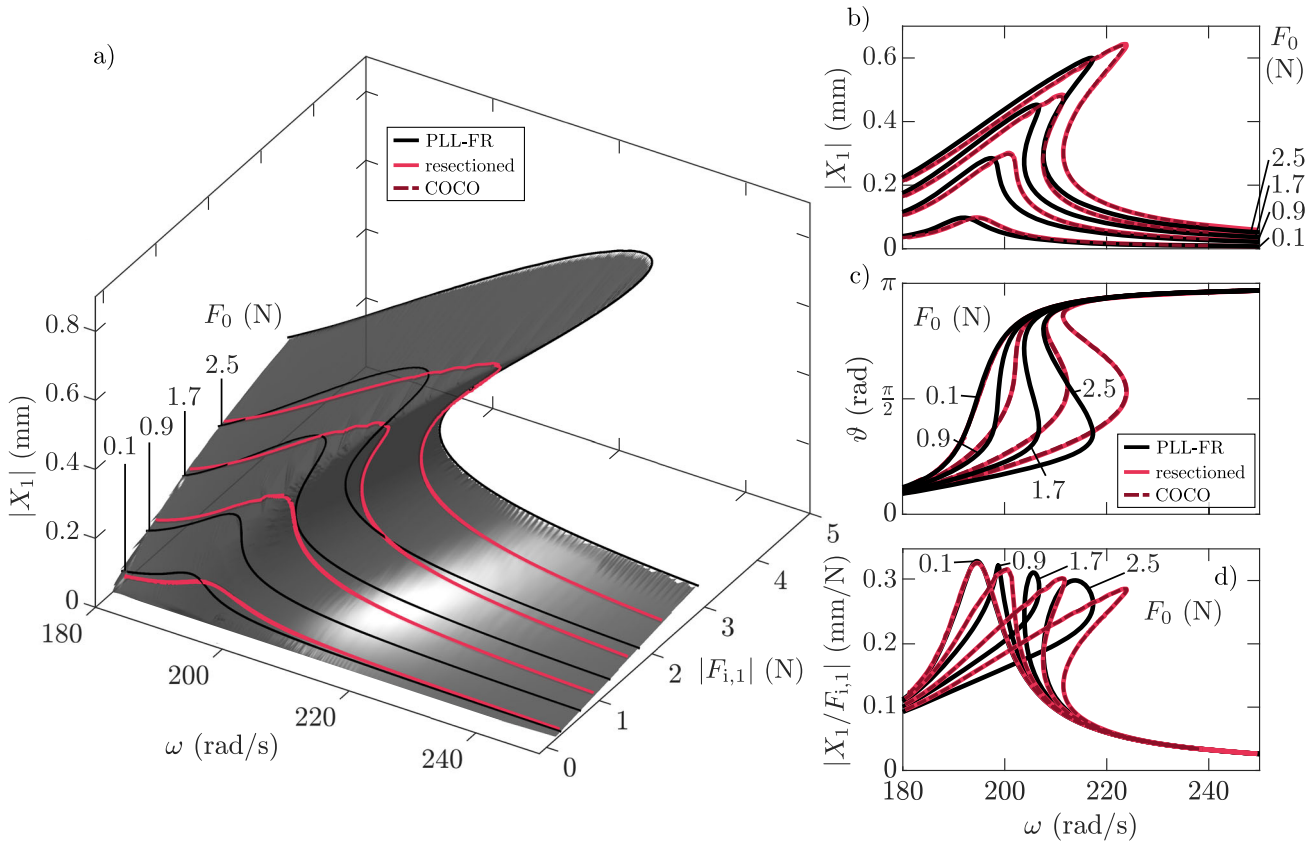

Fig. 4 NLFR surface from PLL-FR tests, based on numerical simulations. **a** Response amplitude surface; **b–d** difference between the numerical PLL-FR tests and the resectioned NLFR curves visible for the amplitude, phase and input force normalized amplitude of the oscillation. Results are compared to the continuation solution for the equivalent 1 DoF oscillator by COCO

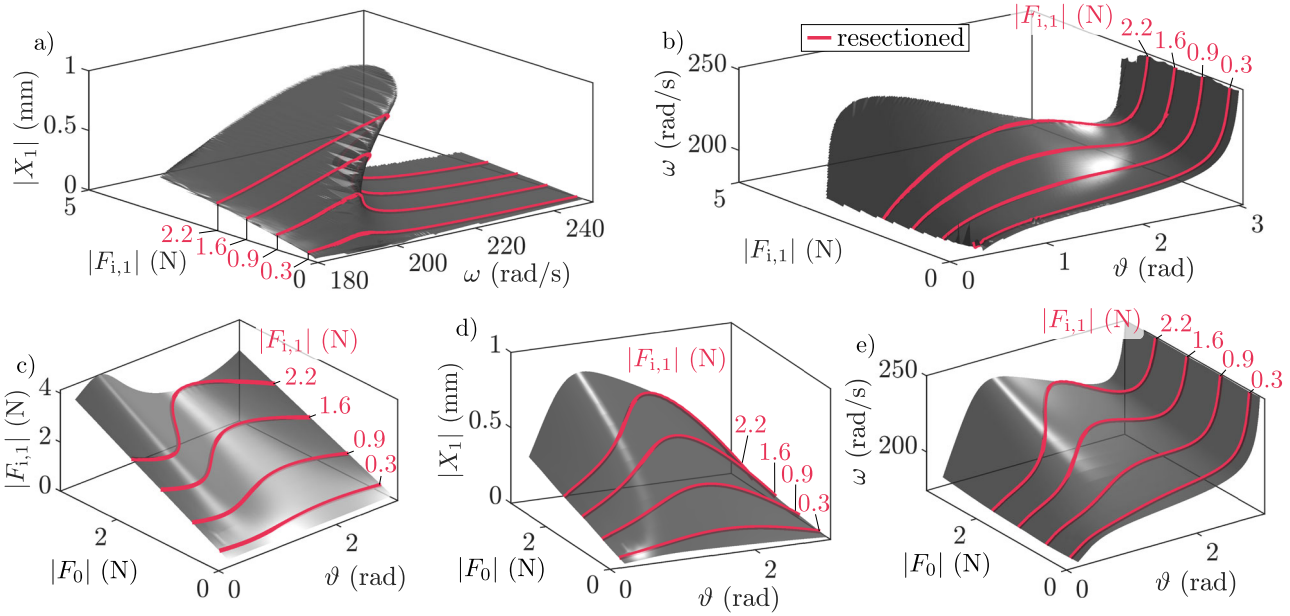

Fig. 5 NLFR surfaces from the PLL-FR tests (numerical simulations). **a**, **b** Direct and **c–e** input signal-based interpolations

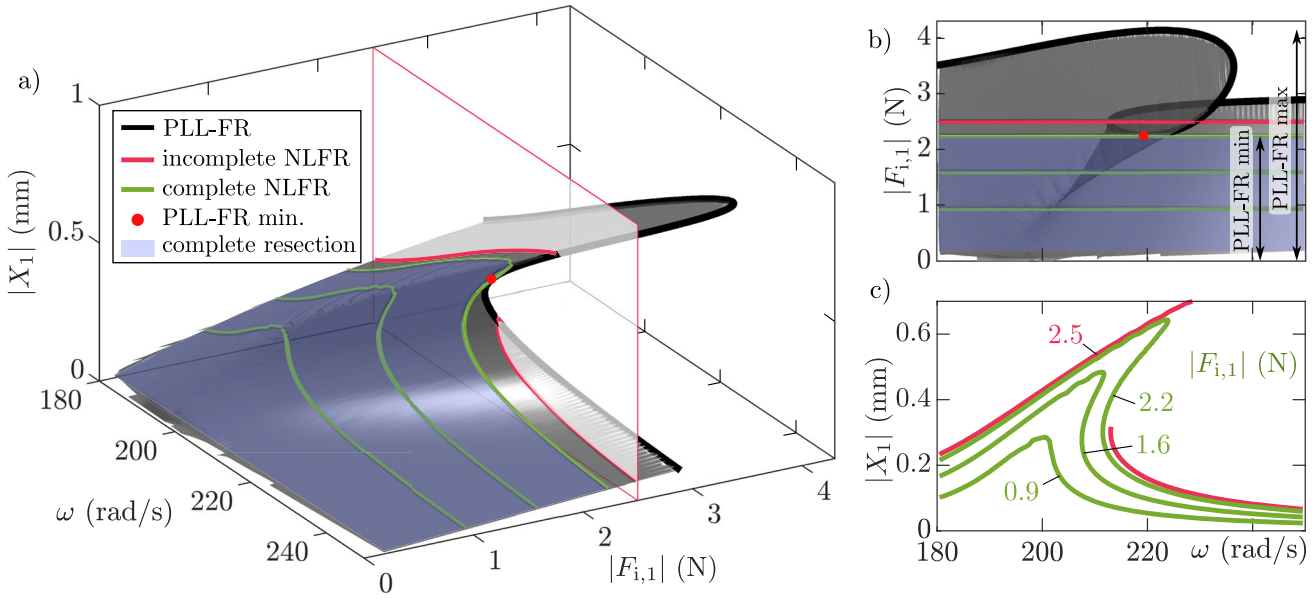

Fig. 6 **a**, **b** Demonstration of the NLFR surface corresponding to complete response curve extraction (blue); **c** resectioned NLFR curves. (Color figure online)

curve extraction. The second approach is to create the functions $F_{i,1}(F_0, \vartheta)$, $X_1(F_0, \vartheta)$ and $\omega(F_0, \vartheta)$, where F_0 and ϑ are input values. Then, the constant input force amplitude $F_{i,1}$ sections are found through the mentioned appropriate F_0 and ϑ inputs. Finally, the ω and $|X_1|$ values corresponding to the constant input force amplitude $F_{i,1}$ sections can be extracted by substitution of the correct input values, see Fig. 5c–e (driving force F_0 amplitude-based interpolation) [29].

Although the resectioning strategy can be effective, looking carefully at Fig. 6 shows that the resectioning can lead to incomplete NLFR (red) curves. This is due to the input force drop-off phenomenon at resonance, leading to the inability to collect sufficient data in some part of the $\omega - F_{i,1}$ domain. This limitation is defined by the minimum of the PLL-FR test (red dot in Fig. 6), corresponding to the highest driving force amplitude F_0 (black line in Fig. 6). Complete NLFR curve extraction is only possible below this minimum value, corresponding to the blue area in Fig. 6a and b. This area shrinks as shaker-structure interaction gets more prominent, meaning more and more PLL-FR tests are required to enlarge the domain for complete resectioning.

The time required to trace NLFR surfaces with the desired input force amplitude $|F_{i,1}|$ range increases significantly as the coupling effect intensifies due to shaker-structure interaction. Interpolating NLFR surfaces in such cases also becomes more challenging. To address this, PLL-FR tests are replaced by PLL-IF tests to reach the incomplete segments more efficiently, when the time consumption of PLL-FR tests increases above that of the PLL-IF tests. Therefore, we suggest prioritising the PLL-IF method when the input force variation is large and the complete NLFR curve extraction is challenging within the range of interest.

To ensure complete NLFR surface tracing, up to the desired input force amplitude, PLL-IF testing is recommended. This method involves locking the phase at various values and gradually increasing the driving force signal until the desired maximum input force amplitude is reached, hence the name phase-locked loop input force sweeps (PLL-IF). This process can be repeated for multiple phase lag ϑ values within resonance. The measured PLL-IF curves trace the NLFR surface with complete resectioning, as in Fig. 7. Panel b) confirms that the PLL-IF curves reach the same maximum input force amplitude, ensuring that resectioning the whole NLFR surface leads to complete NLFR curves. Panel c) compares this approach to the COCO solution, showing a perfect match. Although PLL-IF testing typically requires more time than tracing the NLFR surface with PLL-FR tests, it guarantees complete NLFR curve extraction, making it the preferred method in cases of stronger shaker-structure interaction. Note that for mapping the entire NLFR surface of interest, many PLL-IF tests must be carried out to cover a sufficient phase lag ϑ range, regardless of the coupling effect magnitude. In contrast, only a few PLL-FR tests have to be initiated at a lower level of coupling effects. At higher levels, the number of necessary PLL-FR tests exceeds the number of PLL-IF tests.

In summary, the following guidelines recommend the most suitable methods for extracting complete NLFR curves based on the magnitude of the coupling effect:

– **low coupling effect (method 1):**

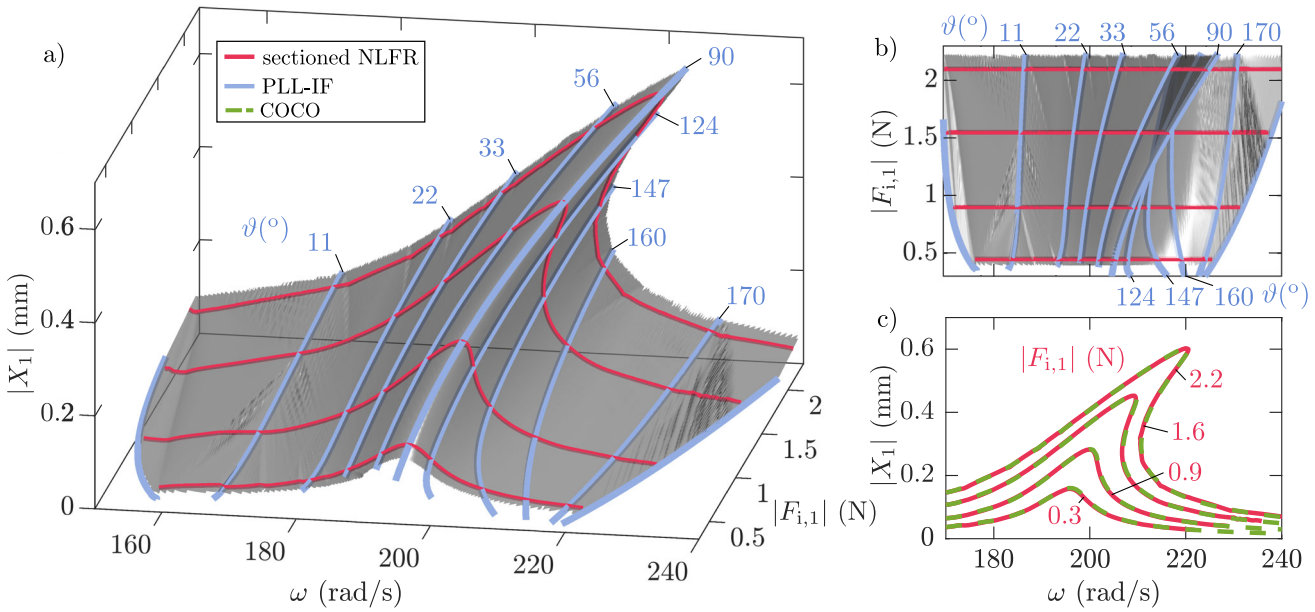

Fig. 7 **a** NLFR surface using the PLL-IF approach, **b** along with the resectioned NLFR curves, and **c** compared to the continuation solution by COCO

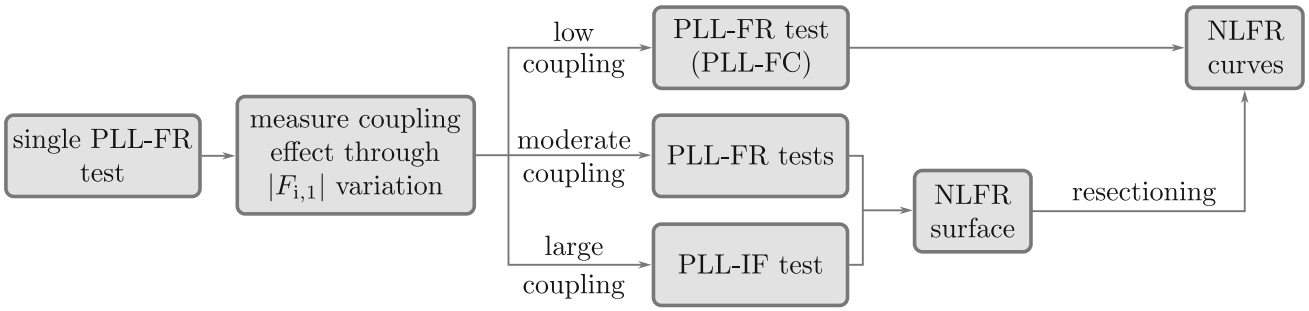

Fig. 8 Proposed measurement process for choosing the appropriate testing technique for the extraction of the NLFR curves. We consider low coupling where force-controlled PLL (PLL-FC) can be performed; however, in this case, PLL-FR can also be performed. **PLL-FR**: Experimental continuation of NLFR curves, where the phase lag ϑ is continuously varied at constant driving force amplitudes F_0. **PLL-IF**: Experimental continuation of $F_{i,1}$-X_1 curves, where the driving force amplitude F_0 is continuously varied at constant phase lags ϑ. Note that by continuously increasing F_0, the input force amplitude $F_{i,1}$ is assumed to increase as well

  - conditions: the input force amplitude deviation during PLL-FR tests is negligible,
  - technique: PLL-FR test without resectioning,
- **moderate coupling effect (method 2):**
  - conditions: the input force amplitude deviation during PLL-FR tests is significant, and complete NLFR extraction can be effectively executed by increasing the output signal amplitude,
  - technique: PLL-FR test with resectioning of the interpolated NLFR surface,
- **large coupling effect (method 3):**
  - conditions: the input force amplitude deviation during PLL-FR tests is significant, and complete NLFR extraction through PLL-FR tests is not feasible or time-consuming,
  - technique: PLL-IF test with resectioning of the interpolated NLFR surface.

The procedure for selecting the appropriate approach and extracting the NLFR curves is summarised in the flow chart shown in Fig. 8. Note that the presented numerical example (1) falls into the moderate coupling effect category. Although there are parts of the NLFR surface that include incomplete data sets, additional PLL-FR tests can easily fill those gaps. Note that a comprehensive picture with all methods presented on the same NLFR surface can be found in the next section, in Fig. 10a–c.

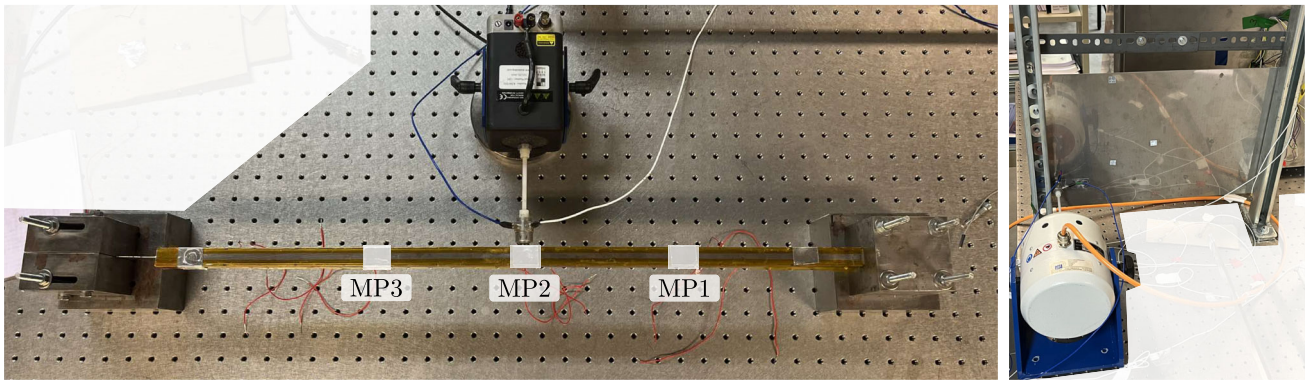

Fig. 9 Measurement setups. Case 1—nonlinear beam structure (on the left). Case 2—fixed metal plate (on the right)

The differentiation between methods 1, 2, and 3 should be guided by on-site engineering decisions, taking into account the available resources. For a specific case, thresholds can be defined to distinguish different levels of coupling: less than 5% deviation for low, less than 50% deviation for moderate, and more than 50% deviation in input force for large coupling. Here, the force deviation is defined as the reduction of the input force amplitude relative to a suitably chosen off-resonance ideal input force amplitude. For cases of large coupling, the PLL-IF method should be applied, as PLL-FR tests would either fail or require excessive time. Below this threshold, PLL-FR can reliably provide accurate NLFR surfaces without the need for input force control. The rationale for introducing the low coupling case is twofold. First, in this regime there is no need to perform resectioning of NLFR surfaces to obtain NLFR curves. Second, low coupling ensures that PLL-FC performs adequately, since the force control has sufficient margin relative to the shaker power to counteract the mechanical coupling between the structure and the shaker.

4 Measurement technique demonstration: shaker—structure interaction

Vibration testing of nonlinear structures is inherently affected by the coupled dynamics between the shaker and the structure [13, 41]. This section illustrates this phenomenon and presents the proposed integrated technique applied to two cases: a nonlinear beam (case 1) and a fixed metal plate (case 2), as shown in Fig. 9. Additionally, the force-controlled PLL-FC method is compared to measured data, highlighting deviations in the input force amplitude under strong shaker-structure interaction. Note that all three methods (PLL-FR, PLL-IF, and PLL-FC) trace the same NLFR surface; however, they do not necessarily maintain a constant forcing amplitude during the measurements.

4.1 Experimental setup

The measured structure for ***case 1*** consists of a monolithic steel nonlinear beam (14 mm × 14 mm × 700 mm) with a thin lamina ending (0.5 mm × 14 mm × 40 mm) that is clamped at the end, as shown in Fig. 9. The hardening nonlinearity of the structure is due to a thin lamina (and also to the clamping).

An electrodynamic shaker (Modal Shop K2007E01) was connected to the beam through a plastic stinger with a diameter of 5 mm and a length of 63 mm. An impedance head (Dytran 5860B) with a signal conditioner (PCB 482C) was glued to the beam, ensuring the continuous recording of the input force and response acceleration $\ddot{x}_2(t) =: \sum_{l=-\infty}^{\infty} A_l \mathrm{e}^{\mathrm{i}l\omega t}$ regarding (1) at the driving point.

The phase-locked loop frequency sweep (PLL-FR) of the integrated technique was realised using a real-time controller unit (dSPACE MicroLabBox) with the sampling frequency set to $\omega_\mathrm{s} = 10$ kHz for both output and input signal processing. The PI controller gains were set to $k_\mathrm{P} = 50$ 1/s and $k_\mathrm{I} = 100$ 1/s^2. For creating force-controlled phase-locked loop (PLL-FC) tests, the force controller could be turned on with the integral gain $k_{\mathrm{I,F}} = 5$ 1/s. The adaptive filter parameter was set to $\gamma = 0.01$ to ensure the sufficient continuation of the phase lag. We note that the phase lag of the measured input force at the impedance head might differ from the one from the driving force signal due to the apparent coupling in the structure, also shown in [13].

The measured structure for ***case 2*** consists of a metal plate, fixed on two sides, with dimensions of (500 mm × 300 mm × 0.5 mm). The nonlinearity comes from the local stretching of the plate and the boundary constraints (contact stiffening/softening at the fixture).

An electrodynamic shaker (Tira TV 51075) was connected to the plate through a 5-mm diameter plastic stinger. A laser Doppler vibrometer (Polytec NLV-2500) was set up perpendicular to the metal plate to measure the response velocity at a certain point on the plate. Otherwise, the data acquisi-

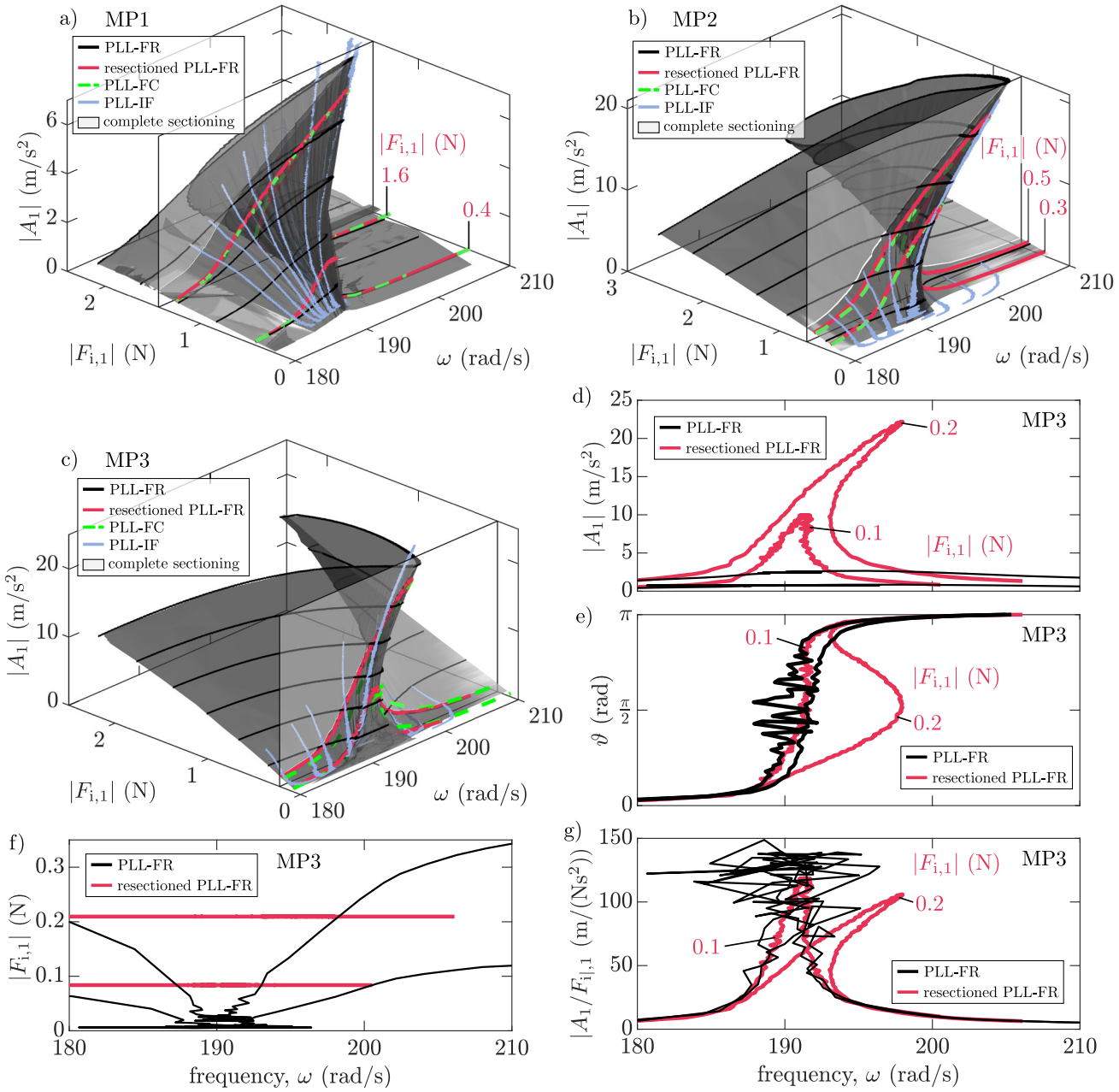

Fig. 10 PLL-FR (frequency-sweep), PLL-IF (input force-sweep) and PLL-FC (force-controlled) tests for the three measurement points (MP1-3). **a–c** Comparison of the methods; **d–g** NLFR, phase lag, input force amplitude and input force-normalized NLFR related to the nonlinear resonance for MP3

tion and equipment were the same as for case 1. The control gains for the PLL-FR were $k_P = 6$ 1/s and $k_I = 2$ 1/s^2. The adaptive filter gain was the same as for case 1.

Note that setting up these structures consistently is crucial. It is known that small changes in the boundary conditions can result in significant differences in the results of testing nonlinear structures [2, 31].

4.2 Experimental demonstration: shaker—beam structure

The NLFR curve extraction of the ***case 1*** structure is demonstrated in this section for three measurement points (MP's in Fig. 9). The varying magnitude of the coupling effect is evident as the shaker is repositioned along the tested beam. Each measurement point was evaluated using the three methods of the integrated technique and compared to PLL-FC testing. The most suitable method for each point was iden-

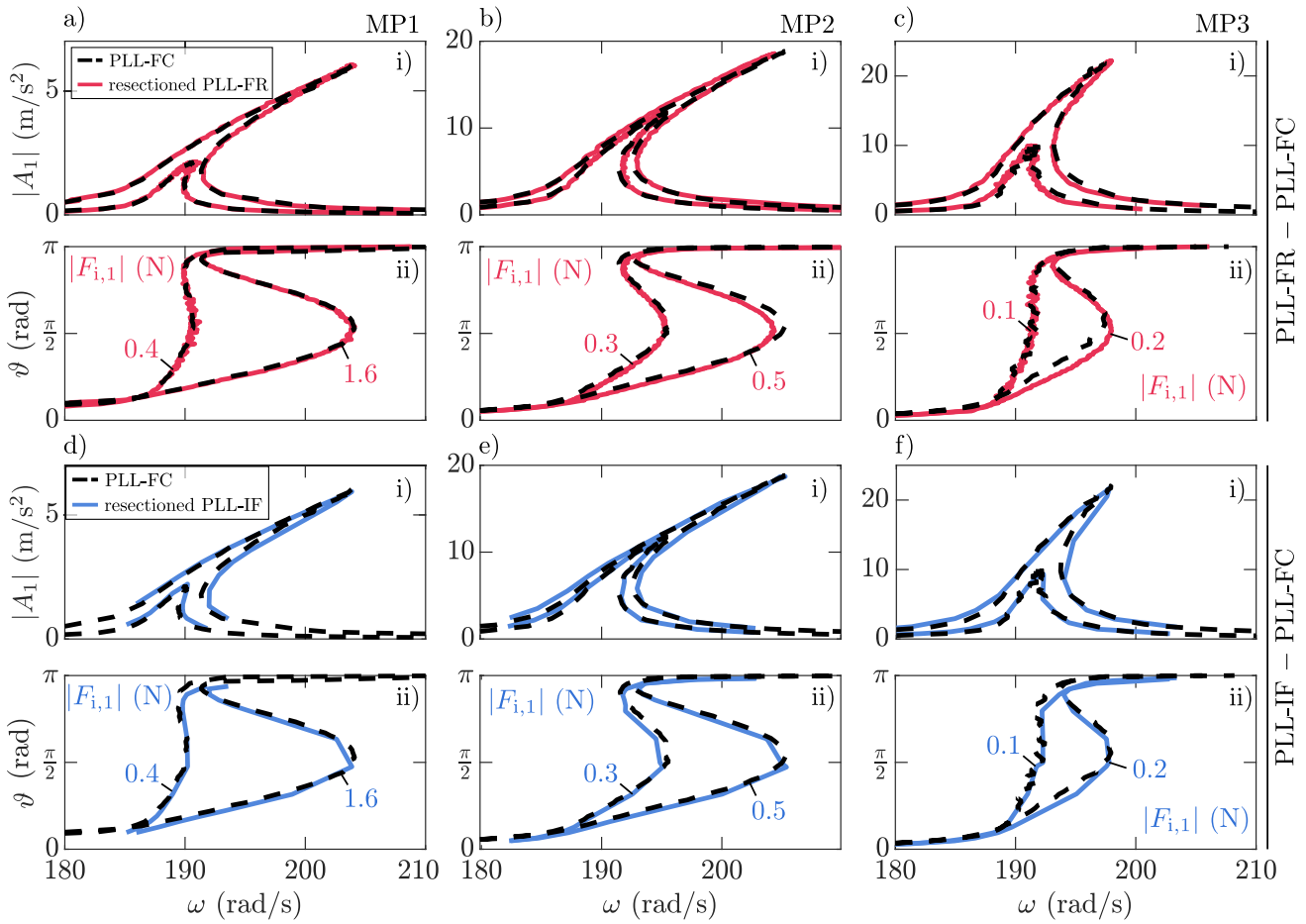

Fig. 11 The proposed PLL methods applied to the three measurement points. **a–c** comparison between the PLL-FC (force-controlled) and resectioned PLL-FR curves; **d–f** comparison between the PLL-FC and the sectioned PLL-IF (input force-sweep) curves. (i–ii) NLFR and phase lag diagrams of the nonlinear resonance

tified. Note that executing all measurement methods is not necessary; this was done here for demonstration purposes. A proper approach can be selected based on the guidelines in Sect. 3. Note that preliminary frequency sweeps are essential to identify the frequency range of the nonlinearity and to roughly determine the phase characteristics of the resonance. This is particularly important in cases with high modal density, where the phase can exceed $\vartheta = \pi$ rad and exhibit complex behavior that must be properly tracked during any PLL-FR test.

Figure 10 presents the results of the PLL-FR approach. All cases exhibit a significant variation in the forcing amplitude (MP1: 32%, MP2: 79%, MP3: 91%), indicating that the NLFR surfaces must be resectioned. Additionally, the boundary of the complete NLFR curve extraction can be drawn as noted with a white plane Fig. 10, for every MP. This plane is a boundary in the input force amplitude. Above this amplitude, the NLFR curves are incomplete. The drawn boundaries at significantly low forcing amplitudes suggest that for MPs 2 and 3, the phase-locked loop input force-sweep (PLL-IF) method would be more effective (large coupling case). The corresponding PLL-FR curves are nearly horizontal at resonance, signifying that a large number of PLL-FR tests with high driving force signal amplitudes were required to trace the surface effectively. Figure 10d illustrates the extreme distortion of the NLFR curves for MP3, further supporting the use of the PLL-IF method if necessary. Moreover, as the coupling effect increases, the signal-to-noise ratio at resonance becomes unacceptable for the PLL-FR tests in panels e-g). As demonstrated in Fig. 10f, the actual input force amplitude drops so much that the response amplitude of the structure becomes comparable to the noise. This results in a noisy resectioning of the measured NLFR surface, as Fig. 10e and g show. Of course, other sources of noise can also affect the extracted NLFR curves that are discussed in [12]. However, the additional noise to these systems is beyond the scope of the present study.

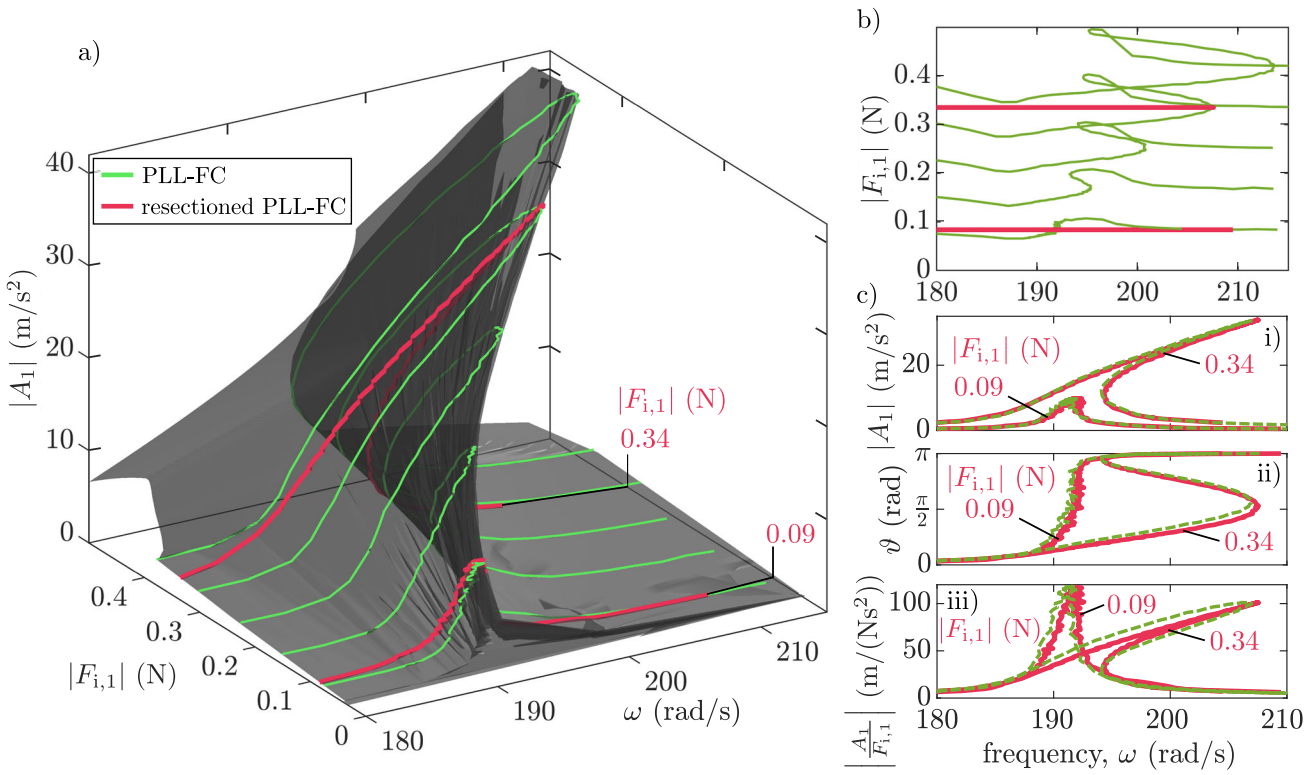

Fig. 12 Forcing amplitude deviation when using PLL-FC (force-controlled) for large coupling effects, at MP3. **a**, **b** Resectioning for the PLL-FC case; **c** comparison of the resectioned and raw PLL-FC tests

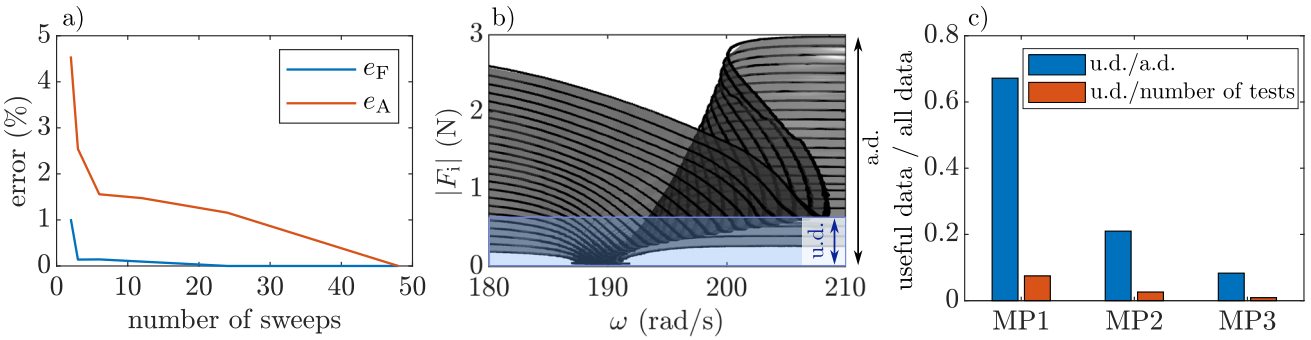

Fig. 13 Quantitative analysis of the PLL-FR approach. **a** relative error for approximating the NLFR curves regarding the number of PLL-FR tests to trace the surface; **b**, **c** useful data (u.d.) for the extraction of complete NLFR curves compared to the available (all) data (a.d.). This comparison shows the rapid growth in the number of PLL-FR tests as the shake-structure interaction gets more prominent

The NLFR surface can also be traced using the PLL-IF method, as shown in Fig. 10. Its advantages include a controllable maximum input force amplitude (without any force controller) for resectioning and fewer tests required compared to the PLL-FR approach, especially in cases with significant coupling effects. Note that the locked phase lags ϑ must be spaced more densely, particularly near 0 rad and π rad, as the dynamics change rapidly around these values. In the close vicinity of $\vartheta = \pi/2$ rad, all PLL-IF sweeps approximately give the phase resonance (backbone curve), due to the input force drop-off phenomenon (extreme drop in Fig. 10f).

Force-controlled PLL-FC tests were also performed on all measurement points within a region where the input force amplitude was controlled sufficiently. Figure 11 presents the comparison, starting with the PLL-FR tests (panels a to c) and followed by the PLL-IF tests (panels d to f). All results align well with the PLL-FC tests, confirming the accuracy of the proposed technique. This demonstrates that PLL-FC can reliably be replaced by the methods outlined in the proposed

guidelines. Consequently, there is no need to include a force controller, which requires stabilization with effective control gains.

Even if a force controller is used for the execution of PLL-FC tests, significant deviation in the input force amplitude can still occur due to the insufficient control scheme, as demonstrated in Fig. 12. As the coupling effect grows, the deviation in the input force amplitude grows with it, similar to the simple PLL-FR tests. Of course, the traced surface can be resectioned for the PLL-FC tests as well, but it eliminates the purpose of the force controller. Moreover, force controllers can be invasive, especially with apparent shaker-structure interaction. Although the NLFR curves and the raw response curves from the PLL-FC tests have only a small visible deviation for this case, the significance of this difference can be important, or the difference can be much larger for other cases. Additionally, the deviation is more prominent if the input force-normalized curves are considered (Fig. 12d). Therefore, we suggest using the proposed technique even if the PLL-FR is replaced by the PLL-FC method.

Finally, quantitative data can be derived from the tests to establish guidelines on the approximate number of measurements required for the PLL-FR tests. First, the relative error of the resectioned PLL-FR curves is calculated in comparison to the PLL-FC results. Note that the force-controlled (PLL-FC) NLFR curve recording for MP1 does not show significant deviation in the input force amplitude. Therefore, we can use it as a benchmark for the error estimation. Formulation of the relative error for both the amplitude e_A and frequency e_F is given as

$$
\begin{aligned}
e_\mathrm{A} &= \sum_{i=1}^{N} \left| \frac{|A_{1,\text{PLL-FR},i}| - |A_{1,\text{PLL-FC},i}|}{|A_{1,\text{PLL-FC},i}|} \right|, \\
e_\mathrm{F} &= \sum_{i=1}^{N} \left| \frac{\omega_{\text{PLL-FR},i} - \omega_{\text{PLL-FC},i}}{\omega_{\text{PLL-FC},i}} \right|,
\end{aligned}
\tag{12}
$$

where N is the number of sampling points in the resectioned NLFR curve, $|A_{1,\text{PLL-FR},i}|$ and $|A_{1,\text{PLL-FC},i}|$ are the acceleration amplitudes of the resectioned NLFR curve and PLL-FC test, respectively. Similarly, $\omega_{\text{PLL-FR},i}$ and $\omega_{\text{PLL-FC},i}$ are the angular frequencies of the resectioned NLFR curve and PLL-FC test, respectively. Note that the i^{th} ($\omega_{\text{PLL-FC},i}$, $|A_{1,\text{PLL-FC},i}|$) point is the closest to ($\omega_{\text{PLL-FR},i}$, $|A_{1,\text{PLL-FR},i}|$) within its branch (e.g. upper branch point can be matched only with an upper branch point). Figure 13a shows that the NLFR curves can be extracted with a relatively low number of PLL-FR tests. This suggests that using PLL-FR tests instead of PLL-FC tests may be more advantageous due to lower measurement costs and the elimination of determining sufficient control parameters. However, the authors still suggest aiming for a significantly large number of curves within the region, where complete NLFR curve extraction is possible. On the other hand, we limit the boundary of the complete NLFR curve extraction by using the PLL-FR approach, see Figs. 13b and 10. The PLL-IF method can be effectively used for avoiding incomplete NLFR curve extraction.

Table 2 Error of the resectioned PLL-FR and PLL-IF test compared to the PLL-FC approach at $|F_{\mathrm{i},1}| \in \{0.3,\ 0.4, 0.5\}$ N

PLL-FR		PLL-IF	
e_F (%)	e_A (%)	e_F (%)	e_A (%)
0.0262	0.3549	0.065	3.529
0.0384	0.4131	0.0351	0.4501
0.0133	0.4567	0.0852	0.9525

The tests were conducted at MP2

The error of the resectioned PLL-FR and PLL-IF methods is then calculated at three constant forcing levels ($|F_{\mathrm{i},1}| \in \{0.3,\ 0.4,\ 0.5\}$ N) at MP2 (large coupling effect) by comparing the two techniques to PLL-FC tests. Using (12), Table 2 was generated, showing low error for both approaches. This reinforces our proposition to be applicable for structures with apparent large coupled effects.

Based on the observations above and the proposed technique, the following conclusions can be drawn regarding the tests in this section. MP1 must be measured by method 2, as the input force amplitude deviation is significant. For MP2 and MP3, the missing data from the traced NLFR surface, leading to incomplete NLFR extraction, is considerably high, classifying these as large coupling cases. In that classification method 3 must be used for efficient complete NLFR extraction. Therefore, we recommend using the resectioned PLL-FR method for MP1 and the PLL-IF method for MP2 and MP3.

4.3 Resectioning with high modal density: metal plate

This section demonstrates the capabilities of the integrated methodology for a structure with higher modal density. The same setup was used in [29], and we used information therein to select intricate nonlinear resonances. Note that the visual interpretation of the measurements was created through the velocity response $\dot{x}_2 =: \sum_{l=-\infty}^{\infty} V_l \, \mathrm{e}^{\mathrm{i}l\omega t}$ due to the laser-based measurements.

First, a well-separated primary resonance with hardening characteristics between 165 and 180 rad/s was considered. PLL-FR and force-controlled phase-locked loop (PLL-FC) tests were carried out with increasing output signal amplitudes. The results are shown in Fig. 14a–c. Both interpolating and resectioning the NLFR surface could be done with relative ease. However, panel c) shows that the force controller in the PLL-FC failed to hold a constant input force level at

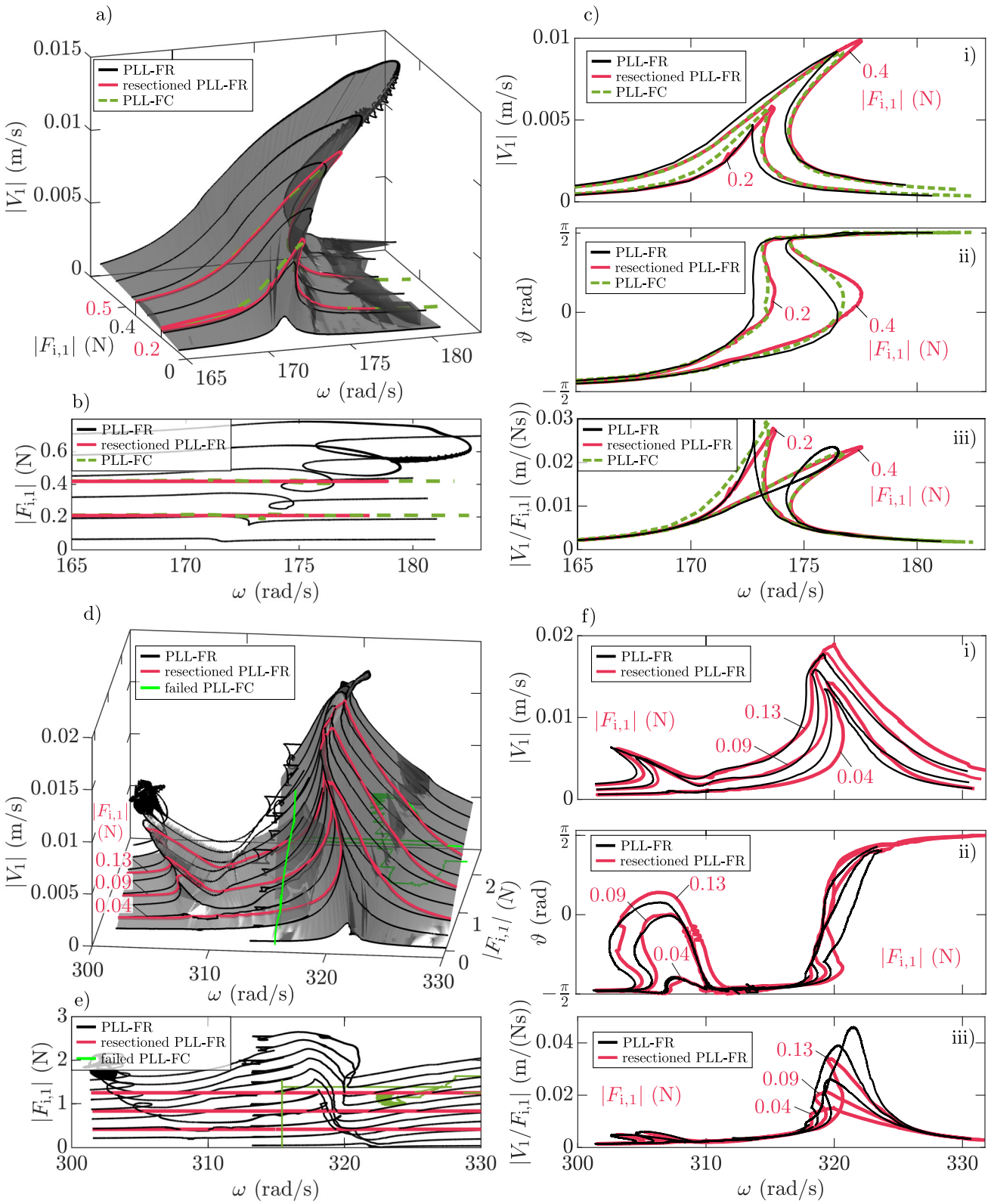

Fig. 14 PLL-FR tests combined with resectioning the NLFR surface for case 2. **a**, **b** interpolated surface; **c** resectioned NLFR curves for the PLL-FC and PLL-FR tests (165–180 rad/s); **d–f** resectioned NLFR curves for the PLL-FR test (300–330 rad/s); the PLL-FC approach was highly unstable at higher input force amplitudes for these resonances

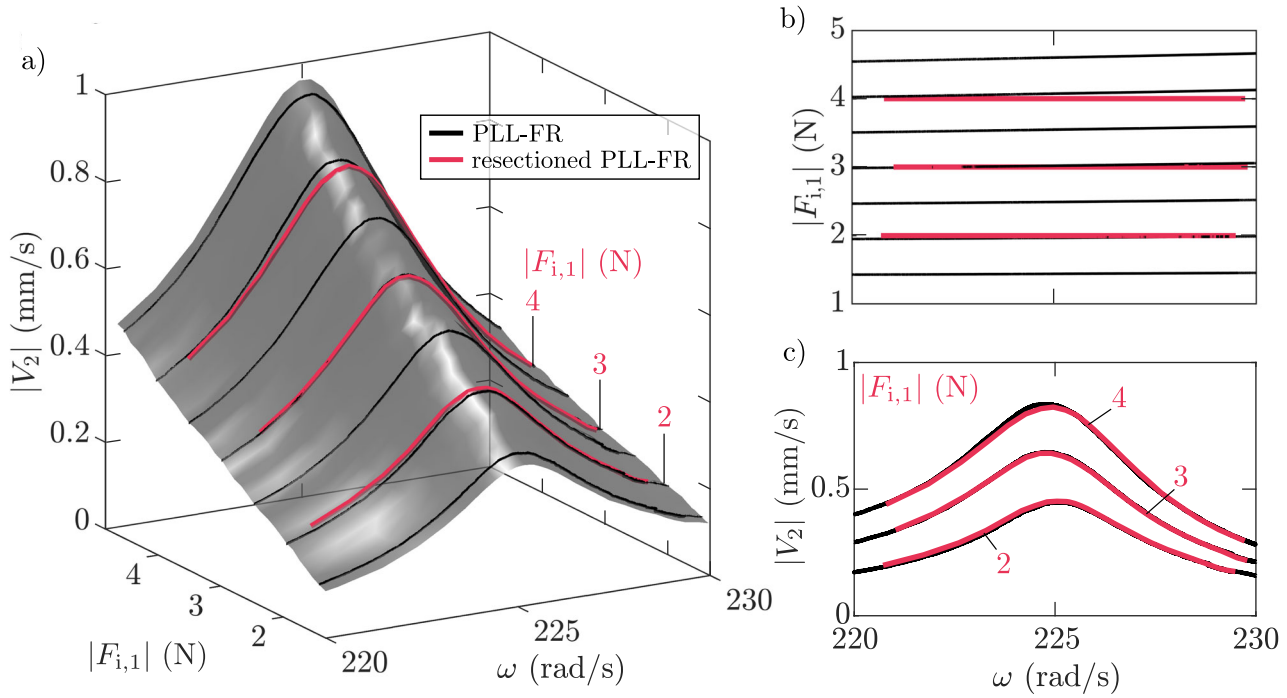

Fig. 15 PLL-FR tests for the 2:1 superharmonic resonance at 225 rad/s. **a**, **b** interpolated NLFR surface; **c** resectioned NLFR curves compared to the PLL-FR tests

resonance, giving slightly different results from the NLFR curves. Again, a force controller can be used but has to be treated with caution.

Then, the frequency range 300–330 rad/s comprising two closely-spaced resonances was targeted. PLL-FR tests were carried out on both resonances separately. The reason is that the target phase lag has to be reset between the two resonances. The results can be seen in Fig. 14d–f. Interestingly, the separately measured resonances could be easily connected after the tests. While interpolating the surface and extracting the NLFR curves provides a detailed view of the underlying nonlinear behavior, we emphasize that the execution was challenging. First, the PLL-FR method itself encounters difficulties with closely spaced vibration modes due to phase lag distortion, as seen in Fig. 14f. Surface fitting cannot be applied to the entire surface due to the repeated phase lag pattern at each resonance. As a result, interpolation and sectioning must be performed separately for each resonance and then combined. It is important to note that the interpolation can be challenging; however, using a denser measurement grid and advanced interpolation techniques can help address this issue. As an example, kriging [3, 22] can be used as a more sophisticated tool, using Gaussian process regression for interpolating the surface. Additionally, the authors were unable to effectively tune the force controller for this case, highlighting the potential of the proposed approach.

We also explored the experimental extraction of harmonics by targeting the 2:1 superharmonic resonance at 225 rad/s forcing frequency. Interestingly, no visible deviation in the forcing amplitude was observed during the PLL-FR tests (Fig. 15b), indicating that this case falls within the low-coupling-effect regime. Although this mode is measured at the same driving point, it leads to a distinct case. While the extraction of NLFR curves can be performed by simply executing the PLL-FR tests (Fig. 15c), we also present the interpolated surface in Fig. 15a. Note that the frequency corresponds to the fundamental harmonic amplitude of the forcing signal, and the response's second harmonic amplitude appears at $2\,\omega$.

In general, resectioning NLFR surfaces measured on structures with higher modal density is both feasible and highly recommended due to uncertainties in the efficiency of the force controller. Additionally, we highlight the detailed insights gained by addressing the coupling effects, compared to the study in [29].

5 Conclusion

This paper presents a technique based on phase-locked loop frequency sweep (PLL-FR) tests for extracting NLFR curves in structures affected by coupling effects originating from a connected shaker. This coupling is often experienced around the resonances, and it is usually eliminated with amplitude

force control; however, the power and/or stroke limitation of the shaker can prevent reaching a uniform forcing level. Three force controller-free methods are introduced, each tailored to different levels of coupling effects. The effectiveness of all proposed methods is demonstrated through numerical and experimental case studies, consistently showing agreement with the expected NLFR curves. We also emphasise that force-controlled phase-locked loop (PLL-FC) tests may exhibit significant deviations in forcing amplitude, posing challenges in determining the control gain required for stabilisation. However, when the appropriate method is selected, PLL-FC tests can be avoided.

The proposed technique is applicable to a wide range of nonlinear structures on which response characterisation is carried out. These structures can include other types of nonlinearities than those shown in this study, where the PLL technique is applicable. Therefore, its potential is to eliminate the use of force controllers in cases where the PLL method can be utilised. However, as modal density increases, interpolation becomes increasingly difficult due to the repeating and distorted phase lag patterns. Future work will focus on improving interpolation techniques to address these limitations.

The technique was also applied to a secondary nonlinear resonance. Interestingly, the tested superharmonic resonance did not exhibit any coupling effects, regardless of the forcing amplitude. This finding reinforces the potential for future studies on secondary resonances.

Author contributions All authors contributed to conceptualising the research. Z.G. and G.R. performed measurement preparation, data collection and analysis. Supervision of the project was ensured by Gaetan Kerschen and Zoltan Dombovari. The first draft of the manuscript was written by Z.G., and all authors commented on previous versions of the manuscript. All authors read and approved the final manuscript.

Funding Open access funding provided by Budapest University of Technology and Economics. Open access funding provided by Budapest University of Technology and Economics.

Data availability The data sets generated and measured during the current study are available from the corresponding author on reasonable request.

Declarations

Conflict of interest The authors declare no conflict of interest.

References

1. Abeloos, G.: Control-based methods for the identification of non linear structures. PhD thesis, University of Liège, Liège, Belgium (2022)
2. Abeloos, G., Müller, F., Ferhatoglu, E., Scheel, M., Collette, C., Kerschen, G., Brake, M., Tiso, P., Renson, L., Krack, M.: A consistency analysis of phase-locked-loop testing and control-based continuation for a geometrically nonlinear frictional system. Mech. Syst. Signal Process. **170**, 108820 (2022). https://doi.org/10.1016/j.ymssp.2022.108820
3. Abeloos, G., Renson, L., Collette, C., Kerschen, G.: Stepped and swept control-based continuation using adaptive filtering. Nonlinear Dyn. **104**(4), 3793–3808 (2021). https://doi.org/10.1007/s11071-021-06506-z
4. Ahlquist, J.R., Carreño, J.M., Climent, H., de Diego, R., de Alba, J.: Assessment of nonlinear structural response in a400m gvt. In: Proulx, T. (ed.) Structural Dynamics, Volume 3, pp. 1147–1155. Springer, New York (2011). https://doi.org/10.1007/978-1-4419-9834-7_101
5. Alijani, F., Amabili, M., Ferrari, G., D'Alessandro, V.: Nonlinear vibrations of laminated and sandwich rectangular plates with free edges. Part 2: experiments and comparisons. Compos. Struct. **105**, 437–445 (2013). https://doi.org/10.1016/j.compstruct.2013.05.020
6. Barton, D., Mann, B., Burrow, S.: Control-based continuation for investigating nonlinear experiments. JVC/J. Vib. Control **18**(4), 509–520 (2012). https://doi.org/10.1177/1077546310384004
7. Dankowicz, H., Schilder, F.: Recipes for Continuation. SIAM (2013)
8. Denis, V., Jossic, M., Giraud-Audine, C., Chomette, B., Renault, A., Thomas, O.: Identification of nonlinear modes using phase-locked-loop experimental continuation and normal form. Mech. Syst. Signal Process. **106**, 430–452 (2018). https://doi.org/10.1016/j.ymssp.2018.01.014
9. Doedel, E.J.: Auto: a program for the automatic bifurcation analysis of autonomous systems. Congr. Numer. **30**(265–284), 25–93 (1981)
10. Ewins, D.: Modal testing: theory, practice and application. In: Mechanical Engineering Research Studies: Engineering Dynamics Series. Wiley (2009)
11. Farago, D., Dombovari, Z.: Experimental study on free vibratory behavior of nonlinear structure. Period. Polytech. Mech. Eng. **63**(2), 91–99 (2019). https://doi.org/10.3311/PPme.12481
12. Gabos, Z., Barton, D.A., Dombovari, Z.: Equation-free bifurcation analysis of a stochastically excited duffing oscillator. J. Sound Vib. **547**, 117536 (2023). https://doi.org/10.1016/j.jsv.2022.117536
13. Gabos, Z., Dombovari, Z.: Open-loop swept frequency response of nonlinear structures subjected to weak coupling. Nonlinear Dyn. 1–18 (2024). https://doi.org/10.1007/s11071-024-10546-6
14. Guckenheimer, J., Holmes, P.: Nonlinear Oscillations, Dynamical Systems, and Bifurcations of Vector Fields, vol. 42. Springer, Berlin (2013)
15. Heylen, W., Lammens, S., Sas, P.: Modal analysis theory and testing. In: Katholieke Universiteit Leuven. Departement Werktuigkunde, Leuven (1997)
16. Hippold, P., Kleyman, G., Woiwode, L., Wei, T., Müller, F., Schwingshackl, C., Scheel, M., Tatzko, S., Krack, M.: An iteration-free approach to excitation harmonization. Mech. Syst. Signal Pro-

cess. **233**, 112732 (2025). https://doi.org/10.1016/j.ymssp.2025.112732
17. Hippold, P., Scheel, M., Renson, L., Krack, M.: Robust and fast backbone tracking via phase-locked loops. Mech. Syst. Signal Process. **220**, 111670 (2024). https://doi.org/10.1016/j.ymssp.2024.111670
18. Jokar, H., Vatankhah, R., Mahzoon, M.: Nonlinear vibration analysis of horizontal axis wind turbine blades using a modified pseudo arc-length continuation method. Eng. Struct. **247**, 113103 (2021). https://doi.org/10.1016/j.engstruct.2021.113103
19. Karaağaçlı, T., Özgüven, H.N.: Experimental modal analysis of nonlinear systems by using response-controlled stepped-sine testing. Mech. Syst. Signal Process. **146**, 107023 (2021). https://doi.org/10.1016/j.ymssp.2020.107023
20. Kerschen, G., Worden, K., Vakakis, A.F., Golinval, J.C.: Past, present and future of nonlinear system identification in structural dynamics. Mech. Syst. Signal Process. **20**(3), 505–592 (2006). https://doi.org/10.1016/j.ymssp.2005.04.008
21. Kleyman, G., Tatzko, S., Wallaschek, J.: Application of experimental continuation to a geometrically nonlinear beam. In: International Conference on Noise and Vibration Engineering, pp. 2387–2399 (2022)
22. Matheron, G.: Principles of geostatistics. Econ. Geol. **58**(8), 1246–1266 (1963)
23. Nayfeh, A.H., Mook, D.T.: Nonlinear Oscillations. Wiley, New Jersey (2008)
24. Noël, J., Kerschen, G.: Nonlinear system identification in structural dynamics: 10 more years of progress. Mech. Syst. Signal Process. **83**, 2–35 (2017). https://doi.org/10.1016/j.ymssp.2016.07.020
25. Noël, J., Renson, L., Kerschen, G.: Complex dynamics of a nonlinear aerospace structure: experimental identification and modal interactions. J. Sound Vib. **333**(12), 2588–2607 (2014). https://doi.org/10.1016/j.jsv.2014.01.024
26. Opreni, A., Vizzaccaro, A., Frangi, A., Touzé, C.: Model order reduction based on direct normal form: application to large finite element mems structures featuring internal resonance. Nonlinear Dyn. **105**(2), 1237–1272 (2021). https://doi.org/10.1007/s11071-021-06641-7
27. Peter, S., Leine, R.I.: Excitation power quantities in phase resonance testing of nonlinear systems with phase-locked-loop excitation. Mech. Syst. Signal Process. **96**, 139–158 (2017). https://doi.org/10.1016/j.ymssp.2017.04.011
28. Ponsioen, S., Pedergnana, T., Haller, G.: Automated computation of autonomous spectral submanifolds for nonlinear modal analysis. J. Sound Vib. **420**, 269–295 (2018). https://doi.org/10.1016/j.jsv.2018.01.048
29. Raze, G., Abeloos, G., Kerschen, G.: Experimental continuation in nonlinear dynamics: recent advances and future challenges. Nonlinear Dyn. **113**(6), 4949–4997 (2025). https://doi.org/10.1007/s11071-024-10543-9
30. Rosenberg, R.: On Nonlinear Vibrations of Systems with Many Degrees of Freedom, pp. 155–242. Elsevier (1966). https://doi.org/10.1016/S0065-2156(08)70008-5
31. Schwarz, S., Kohlmann, L., Hartung, A., Gross, J., Scheel, M., Krack, M.: Validation of a turbine blade component test with frictional contacts by phase-locked-loop and force-controlled measurements. J. Eng. Gas Turbines Power **142**(5), 051006 (2020). https://doi.org/10.1115/1.4044772
32. Shaw, S., Pierre, C.: Normal modes of vibration for non-linear continuous systems. J. Sound Vib. **169**(3), 319–347 (1994). https://doi.org/10.1006/jsvi.1994.1021
33. Sieber, J., Krauskopf, B.: Control based bifurcation analysis for experiments. Nonlinear Dyn. **51**(3), 365–377 (2008). https://doi.org/10.1007/s11071-007-9217-2
34. Sokolov, I., Babitsky, V.: Phase control of self-sustained vibration. J. Sound Vib. **248**(4), 725–744 (2001). https://doi.org/10.1006/jsvi.2001.3810
35. Suhir, E., Vujosevic, M., Reinikainen, T.: Nonlinear dynamic response of a 'flexible-and-heavy'printed circuit board (PCB) to an impact load applied to its support contour. J. Phys. D Appl. Phys. **42**(4), 045506 (2009). https://doi.org/10.1088/0022-3727/42/4/045506
36. Touzé, C., Vizzaccaro, A., Thomas, O.: Model order reduction methods for geometrically nonlinear structures: a review of nonlinear techniques. Nonlinear Dyn. **105**(2), 1141–1190 (2021). https://doi.org/10.1007/s11071-021-06693-9
37. Varoto, P.S., de Oliveira, L.P.R.: On the force drop off phenomenon in shaker testing in experimental modal analysis. Shock. Vib. **9**(4–5), 675674 (2002). https://doi.org/10.1155/2002/675674
38. Wei, Y., Dong, Y., Huang, X., Zhang, Z.: Nonlinearity measurement for low-pressure encapsulated mems gyroscopes by transient response. Mech. Syst. Signal Process. **100**, 534–549 (2018). https://doi.org/10.1016/j.ymssp.2017.07.034
39. Woiwode, L., Krack, M.: Experimentally uncovering isolas via backbone tracking. J. Struct. Dyn. **2**, 122–143 (2024). https://doi.org/10.25518/2684-6500.180
40. Zhang, G., Wang, X., Yang, Z.: Study on excitation force characteristics in a coupled shaker-structure system considering structure modes coupling. Chin. J. Aeronaut. **35**(7), 227–245 (2022). https://doi.org/10.1016/j.cja.2021.11.024
41. Zhou, T., Kerschen, G.: Identification of secondary resonances of nonlinear systems using phase-locked loop testing. J. Sound Vib. **590**, 118549 (2024). https://doi.org/10.1016/j.jsv.2024.118549